Wafer-Scale Manufacturing of Bulk Shape-Memory-Alloy Microactuators Based on Adhesive Bonding of Titanium-Nickel Sheets to Structured Silicon Wafers

Stefan Braun, Niklas Sandström, Göran Stemme *Fellow, IEEE* and Wouter van der Wijngaart *Member, IEEE*

***Abstract*—This paper presents a concept for the wafer-scale manufacturing of microactuators based on the adhesive bonding of bulk shape memory alloy (SMA) sheets to silicon microstructures. Wafer-scale integration of a cold-state deformation mechanism is provided by the deposition of stressed films onto the SMA sheet. A concept for heating of the SMA by Joule heating through a resistive heater layer is presented. Critical fabrication issues were investigated, including the cold-state deformation, the bonding scheme and related stresses and the Titanium-Nickel (TiNi) sheet patterning. Novel methods for the transfer stamping of adhesive and for the handling of the thin TiNi sheets were developed, based on the use of standard dicing blue tape. First demonstrator TiNi cantilevers, wafer-level adhesively bonded on a microstructured silicon substrate, were successfully fabricated and evaluated. Intrinsically stressed silicon dioxide and silicon nitride were deposited using plasma enhanced chemical vapor deposition to deform the cantilevers in the cold state. Tip deflections for 2.5 mm long cantilevers in cold/hot-state of 250/70 µm and 125/28 µm were obtained using silicon dioxide and silicon nitride, respectively. The bond strength proved to be stronger than the force created by the 2.5 mm long TiNi cantilever and showed no degradation after more than 700 temperature cycles. The shape memory behavior of the TiNi is maintained during the integration process.**

***Index Terms*—Adhesive bonding, blue tape, contact printing, microactuator, microelectromechanical systems (MEMS), nitinol, shape memory alloy (SMA), stress layers, titanium-nickel (TiNi), integration, transfer stamping, wafer-scale integration, wet etching.**

I. Introduction

MICROELECTROMECHANICAL systems (MEMS) technology offers a large range of microactuators for specific applications, based on different actuation principles such as electrostatic, piezoelectric, thermal and magnetic actuation [1], [2]. In a comparison of the different microactuators, the shape memory alloy (SMA) actuators offer the highest work density, which exceeds that of other actuation principles by at least an order of magnitude [3]. Examples of SMA microactuation can be found in [4], [5], [6], [7].

The SMA microactuators deploy the shape memory effect, which is the ability of certain materials to 'remember' their initial shape when they are deformed. At low temperatures the SMA material is in the martensite phase (hereafter referred to as cold state). The SMA cantilever will easily deform under stress and will remain deformed after the stress has been removed. Upon heating, the SMA material will change to its austenite phase (hereafter referred to as hot state) and the cantilever will rapidly and completely recover its initial shape. After subsequent cooling, the cantilever will keep its shape until it is deformed again.

Even though there are a number of materials showing the shape memory effect [8], [9], [10], most of the SMA microactuators are based on alloys of Titanium and Nickel (hereafter referred to as TiNi) because of several advantages over other materials. TiNi alloys allow for adjusting the transformation temperatures over a temperature range of typically - 50 °C to 110 °C, only by changing the Ni over Ti ratio of the alloy. Furthermore, TiNi alloys can be fabricated with standard metalworking techniques, they exhibit better shape memory strain performance than other known alloys and they consist only of the affordable elements Nickel and Titanium [11], [12]. The work presented in this paper is based on bulk, cold-rolled TiNi films. However, many of the presented methods are generic and can be applied to other SMA materials.

Despite the advantages, SMA materials are not yet a standard MEMS material, partially due to the lack of proper methods for the wafer-scale and batch-compatible manufacturing and integration of SMA materials with MEMS structures. Previous work on the integration of SMA material in MEMS devices can be summarized in two different approaches. One approach, the hybrid integration, is to fabricate the SMA actuator element and the MEMS structure separately. The bias spring is provided by a mechanical obstruction on the MEMS structure, which deforms the SMA element during the assembly of the SMA element and the MEMS structure [13]. This approach features several advantages such as the use of bulk SMA, which is commercially available in a wide thickness range and therefore allows for adjustable mechanical robustness and reduced material cost. Furthermore, using bending motions generates both large displacement and forces and for SMA thicknesses above 30 µm bending motions in

Manuscript received April 3, 2009; revised July 28, 2009. This work was supported by the European Commission through the sixth framework program. Subject Editor Y. B. Gianchandani.

The authors are with the Microsystem Technology Laboratory, School of Electrical Engineering, The Royal Institute of Technology, 100 44 Stockholm, Sweden (e-mail: stefan.braun@ee.kth.se; Niklas.Sandstrom@ee.kth.se; Goran.Stemme@ee.kth.se; wouter@ee.kth.se).

Color versions of one or more of the figures in this paper are available online at http://ieeexplore.ieee.org.

Digital Object Identifier 10.1109/JMEMS.2009.2035368

the substrate-plane can be realized [3]. However, the required per-component assembly is not batch compatible and results in unacceptable high costs. Batch processing compatibility is provided by another method, the sputtering or evaporation of thin SMA films [4] on the MEMS structure. In this approach, the monolithic integration, the bias spring is provided by the built-in film stress. However, sputtering of SMA is complicated and an annealing of the material at high temperatures is necessary, which implies unwanted interdiffusion processes of the SMA with the substrate. Furthermore, the thicknesses of the sputtered TiNi-films are limited to approximately 20 µm [3] and a recent report states that TiNi-based film sputtering is mostly feasible for thicknesses up to 10 µm only [14]. For completeness it should be mentioned that in a recent report [15] a 30 µm thick film of a ternary TiNi based alloy was achieved by flash-evaporating TiNiCu onto copper substrates, however, the issues of complicated processing and high post-deposition annealing temperatures are still not overcome.

To the authors' knowledge, there are only few reports on wafer-scale integration of bulk SMA sheets with silicon based microstructures. In a previous work [16], a SMA sheet was patterned on wafer-scale and the elements were selectively transferred to single plastic microvalves. However, the cold-state reset was provided by a spacer between the microvalve and the SMA element, which requires pick and place assembly and furthermore the electrical contacting of the SMA was performed using a complicated gap welding process. Another report [17] introduces the wafer-scale integration of pre-strained SMA wires using adhesive bonding and utilizing single-crystalline silicon as cold-state reset. This approach looks promising, however, it addresses the integration of SMA wires instead of SMA sheets.

The present paper introduces a novel concept for both the wafer-scale manufacturing and the integration of robust trimorph bulk SMA microactuators on silicon wafers, circumventing the limitations of the previous methods. The work addresses three key aspects for wafer-scale and batch compatible manufacturing of SMA microactuators based on bulk TiNi. The first is to provide both a batch manufacturing compatible and wafer-scale cold-state reset mechanism and a concept for thermal energy supply. The second aspect is the wafer-scale integration of bulk TiNi with microstructured silicon wafers. The third aspect is the patterning of the TiNi using the very aggressive HF/HNO_3 based etchant. The experimental part of this work focuses mainly on the integration of the TiNi and its cold state reset. Preliminary results are reported in [18]. The technology for the transfer of TiNi sheets to silicon described in this paper is generic and can be used for other metal films.

II. Concept for the wafer-scale Manufacturing of Bulk SMA microactuators

A. Wafer-scale and batch-compatible cold-state reset and thermal energy supply mechanism

The proposed actuator design contains three functional layers (Figure 1a). The first functional layer consists of the bulk SMA sheet.

The second functional layer is a stressed film which deforms the SMA in the cold state and, in contrast to previous

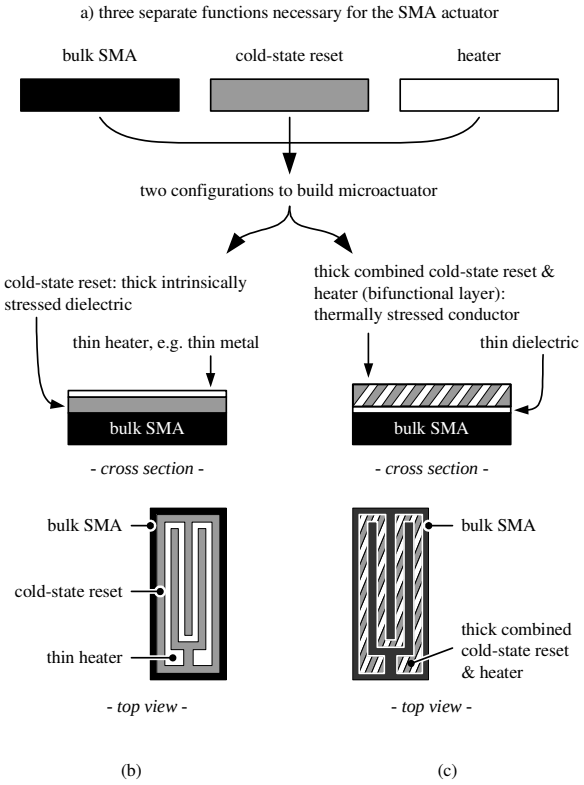

Figure 1. Figure showing (a) an illustration of the functional layers, (b) and (c) the two different proposed configurations of the functional layers.

bulk SMA microactuators, eliminates the need for pick-and-place integration. Besides the batch-compatibility of depositing stressed thin films, this method also allows for tuning the actuator characteristics by the choice of layer thicknesses, material deposition technology and deposition conditions. Depending on these parameters, the stress in the deposited film is either compressive or tensile. Compressive or tensile stresses arise from thermal and/or intrinsic stresses. Thermal stresses result from a mismatch of the coefficient of thermal expansion (CTE) of the deposited layer towards the substrate, whereas intrinsic stresses result from non-uniformities during the film nucleation. When depositing films on a substrate, the intrinsic stresses are often combined with thermal stresses because of the different CTE of the two materials, however, in most cases the intrinsic stress component is much larger than the thermal stress component [19].

The third functional layer is a heating layer to supply thermal energy to the actuator via an indirect heating scheme. The heating layer is a resistive heater, which potentially allows for straightforward electrical contacting and low actuation current. The heater-pattern can be optimized to reduce both thermal gradients along the beam and power consumption. Furthermore, an indirect heater eliminates the need to pattern the bulk SMA for direct heating and thereby eliminates the potential mechanical weakening of the SMA material.

This paper suggests two different arrangements of the cold-state reset and heater layer on top of the bulk SMA layer, differing in the materials and their thicknesses (Figure 1). The first configuration (Fig. 1b) contains a thick and stressed

dielectric layer deposited on top of the SMA and providing the cold-state reset. Examples for a dielectric cold-state reset layer are intrinsically stressed silicon dioxide (SiO_2) or silicon nitride (Si_3N_4) layers deposited by plasma enhanced chemical vapor deposition (PECVD). On top of the dielectric layer a thin electrically conductive layer, typically a metal, is deposited and patterned to form a resistive heater.

The second configuration (Fig. 1c) consists of a thick electrically conductive layer, which combines the functions of cold-state reset and thermal energy supply. This bifunctional layer must be patterned to form a resistive heater. An example of a bifunctional layer is aluminum, sputtered at elevated temperatures and forming a standard thermal bimorph scheme [20]. However, to prevent leakage currents from the bifunctional layer into the SMA the two layers must be electrically isolated by a thin intermediate dielectric layer such as SiO_2 or Si_3N_4.

Whereas a dielectric stress layer allows for tuning the type of stress (tensile or compressive), it typically requires higher deposition temperatures than the metal stress layer. The preferred configuration will depend largely on its process compatibility with the rest of the fabrication sequence of the entire microcomponent in focus.

The presented concept is similar to a standard thermal bimorph actuator using two passive materials with different CTE, such as aluminum on a silicon cantilever. The main differences are that in the presented concept the cantilever itself is the core actuation layer, consisting of the relatively thick TiNi and upon heating it provides the highest work density among the MEMS actuators. In the cold state, the TiNi has a very low yield strength and deforms easily, thus it allows for a high deflection using a relatively thin stressing layer only. Also, due to the SMA effect, the actuators' temperature-deflection curve shows typical hysteresis behavior, as compared to the proportional behavior of a standard thermal bimorph.

B. Wafer-scale integration of SMA sheets

This section describes two concepts for integrating SMA onto structured silicon wafers using adhesive bonding [21] (Figure 2).

The first method (Figure 2a) is the adhesive bonding of a wafer-sized, non-patterned TiNi sheet onto the structured silicon wafer, followed by patterning the SMA sheet to form the actuator structures. We successfully demonstrated this method for the integration of postal stamp sized SMA sheets to silicon [22], but not on 4" wafer scale. Bonding prior to patterning provides the advantage that the two substrates must not be precisely aligned during the bonding, simplifying the bonding step. Furthermore, since the SMA sheet is not patterned it is mechanically robust which simplifies the handling. For testing this approach, a 5 µm thick Benzocyclobutene (BCB) layer was spun on a 30 µm thick TiNi sheet, which was then bonded with the BCB side to a structured silicon wafer. Next, the BCB was hardcured by placing the stack in a wafer bonder for 1h at a temperature of 250 °C and applying a load pressure of 0.8 bar. After the bonding, the stack showed a bowing and the TiNi sheet partially delaminated at the edges,

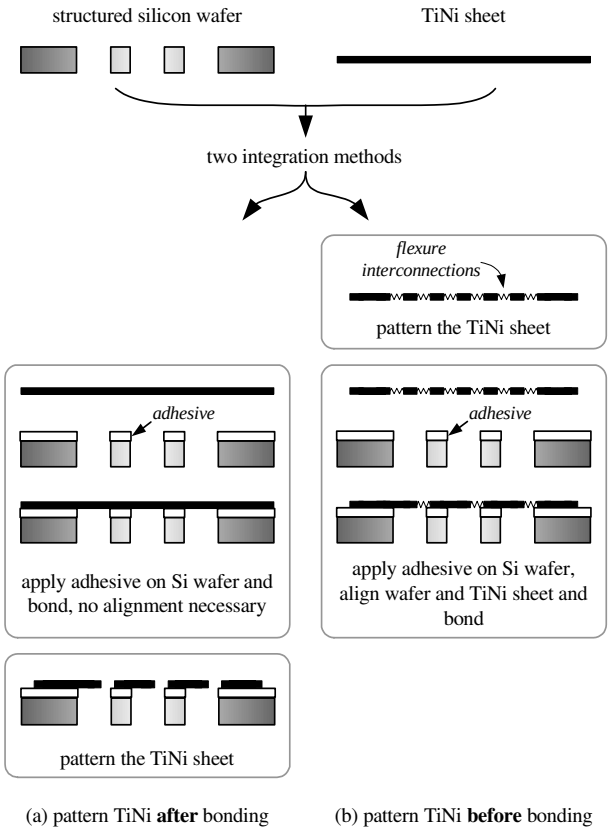

Figure 2. Illustration of the two different methods for integrating TiNi sheets with structured Si wafers, based on a) adhesive bonding prior to the patterning of the TiNi sheet and b) adhesive bonding after pre-patterning the TiNi sheet.

which indicated that the induced thermal stresses upon cooling were too large for the bond interface. Furthermore, when etching the TiNi sheet to create the actuator structures, both the BCB as well as underlying silicon areas were attacked by the aggressive TiNi etchant. The silicon turned black and the BCB swelled heavily, which further decreased the bond quality. Finally, during dicing of the stack the TiNi structures completely delaminated.

Hence, it was concluded that the TiNi sheet must be patterned prior to bonding, which is the second integration method (Figure 2b). This method requires a temporary carrier substrate for the patterning and handling of the SMA sheet as well as an alignment of the sheet and the silicon wafer during the bonding. However, this method offers two major benefits. First, since the SMA sheet is patterned prior to the bonding, the SMA etchant cannot attack any sensitive adhesive layer, silicon or metal structures. Secondly, removing bulk TiNi material allows to address problems related to excessive stress in the adhesive interface after the bonding. Stress in bonded structures is a complex phenomenon [23] and in this work, we did not perform an entire stress analysis. However, we made some first hand assumptions by considering two of the stress components. The first component is the thermal stresses that stem from the different CTE of the two materials. The second component is the shearing stresses caused by the bending moments induced by the thermal bimorph deformation. The bending of the bimorph and thus the shear stress is

reduced when parts of the bulk TiNi material are removed due to mechanically weakening of the TiNi sheet. Yet, to ensure the mechanical integrity of the SMA sheet, the single actuator structures in the pattern must remain mechanically interconnected. To allow the material to release the strain induced by the bimorph bending, the mechanical interconnections between the actuator structures were patterned as flexure interconnections, which deform and thereby absorb parts of the strain (see Fig. 2b). The interconnections can be placed such that they are removed during the final dicing of the wafer.

III. Experiments

A. Cold-state reset layer investigation

Several standard MEMS materials were tested as cold-state reset layer. The tested dielectric layers (Figure 1b) were silicon dioxide (SiO_2) and silicon nitride (Si_3N_4), deposited by PECVD at 300 °C. PECVD allows to deposit dielectric films at moderate temperatures and the deposited films are known to be intrinsically stressed. The tested bifunctional layer (Figure 1c) is aluminum, sputtered onto the TiNi test cantilevers at a temperature of 120 °C. Aluminum is well suited as a thermal bimorph material, using the thermal mismatch between the aluminum and the substrate to induce thermal stresses deflecting the actuator. All the layers were 1 µm thick and deposited on 30 µm thick TiNi sheets. The SMA sheets were then diced into cantilevers with a width and length of 2 mm and 10 mm, respectively.

Then the radius of curvature, R, was measured in both the cold and the hot-state. Figure 3 plots the measured curvatures $\kappa = \frac{1}{R}$ of the cantilevers. The aluminum features tensile stress and both SiO_2 and Si_3N_4 feature compressive stress, resulting in deformations as illustrated in the insets in Fig. 3. The results show that all stress layers deformed the cantilevers in the cold-state. When heated on a hotplate, the TiNi counteracts the cold-state reset and the cantilevers nearly flatten. For Al and Si_3N_4, the hot state deformation was too small to measure. In contrast, the TiNi cantilever cannot fully counteract the SiO_2 cold-state reset layer, which results in a measurable hot-state deformation of the cantilever. However, the large stresses in the SiO_2 layer resulted in a much larger cold-state deformation as compared to the Si_3N_4 and the Al film.

To compare with later test components, the correlated theoretical tip deflections for single clamped 2.5 mm long cantilevers were calculated and are displayed in the right-hand y-axis of the graph in Figure 3. The values indicate a cold-state tip deflection in the range of 155 µm and 80 µm for Al and Si_3N_4, respectively. In the hot-state, these cantilevers would be flat. For SiO_2, a cold-state tip deflection of approximately 180 µm and a hot-state tip deflection of approximately 45 µm is predicted.

For completeness it should be mentioned that the stresses in PECVD Si_3N_4 layers, in contrast to PECVD SiO_2 layers, can be tuned over a wide range by tuning the processing parameters [24]. Furthermore, the intrinsic stresses in Si_3N_4 are more thermally stable as compared to SiO_2 [25], [26], [27].

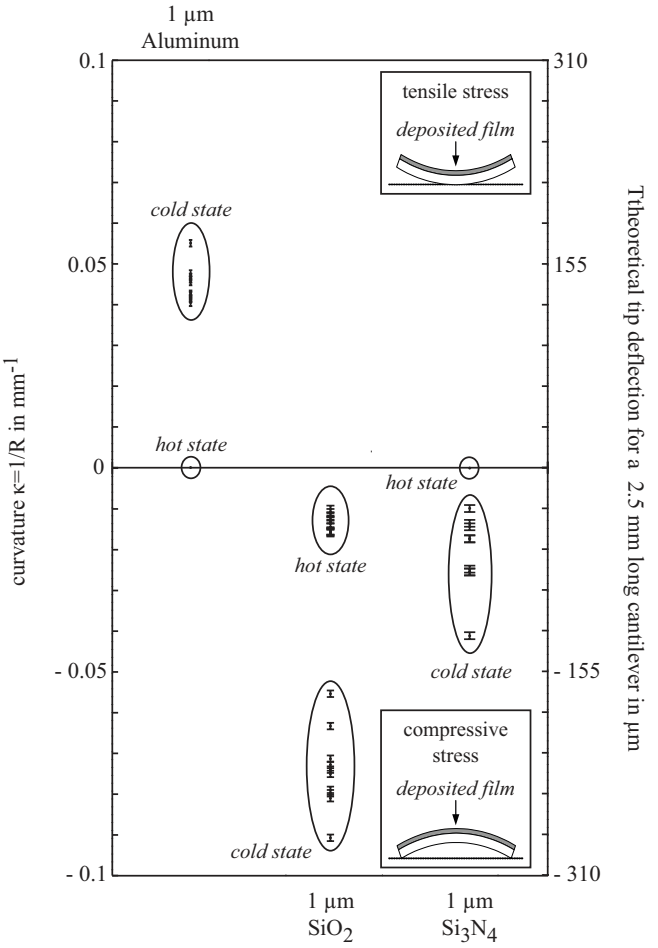

Figure 3. Measurement of the deflection of ten SMA-Al and SMA-PECVD SiO_2 and nine SMA-PECVD Si_3N_4 test bimorph structures in the hot state (90 °C on a hot plate) and in the cold state (at room temperature). The left-hand y-axis displays the measured curvature $\kappa = \frac{1}{R}$ of the TiNi cantilevers on which the layers were deposited. The right-hand y-axis displays the calculated tip deflection if the cold-state reset layers were deposited on 2.5 mm long TiNi cantilevers with the same thickness and material properties. The Al features tensile stress and both SiO_2 and Si_3N_4 feature compressive stress, resulting in different deformation directions.

B. Investigation of bulk TiNi wet etch concentration and masking materials

In most MEMS devices, including those in the current work, the TiNi is wet etched using an aggressive mixture of nitric and hydrofluoric acids in water (HNO_3/HF/H_2O) with varying concentrations to control the etching rate [28]. Such acid-nitric acid-acetic acid (HNA) etch systems have been well characterized to isotropically etch silicon [29], but they also attack many metals and some photoresists [30]. HNO_3 is a powerful oxidizing agent in which the silicon or metal is oxidized. The addition of HF to the solution etches the formed oxide films. However, since the HNA etchant attacks so many materials, a compatible masking material with an acceptable selectivity must be found. Also, the exposure to HF introduces the risk for embrittlement of the TiNi. Previous work indicates, that the selectivity of photoresist allows to etch thin TiNi films if the resist is thick enough [28].

In the present work five materials were tested as masking

Table I
TESTING OF DIFFERENT MASKING MATERIALS FOR THE ETCHING OF A TINI SHEET AT DIFFERENT HNA CONCENTRATIONS.

SMA etch mixture	TiNi	Tested masking materials and their selectivity (mask etch/NiTi etch)				
Vol % HF:HNO_3:H_2O	etch rate $\mu m/min$	pos. resist[a] 1.2 µm	neg. resist[b] 2.8 µm	TiW/Au[c] 50/200 nm	SiO_2[d] 3 µm	Si_3N_4[d] 2 µm
5 : 20 : 75	5	delaminates	deteriorates	not measurable	~1/3	~1/15
5 : 30 : 65	10	delaminates	deteriorates	not measurable	~1/3	~1/15
10 : 20 : 70	20	delaminates	delaminates	not measurable	~1/3	~1/15
10 : 30 : 60	25	delaminates	delaminates	not measurable	~1/3	~1/15

[a] Megaposit SPR 700-1.2; [b] Microresist ma-N 420; [c] sputtered metal layers; [d] PECVD at 300 °C

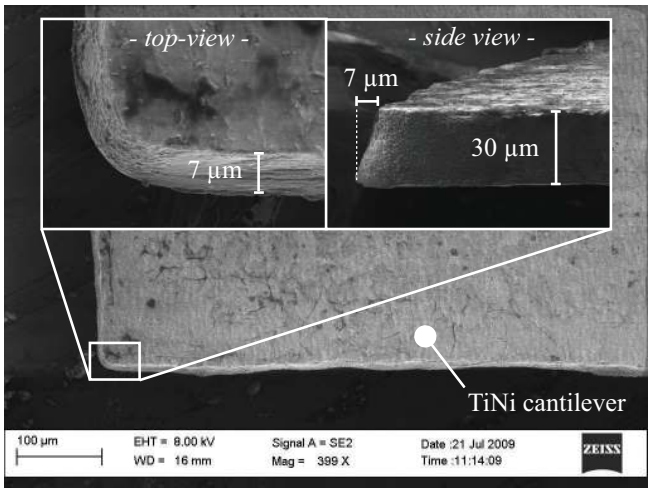

Figure 4. SEM pictures of the corner of a TiNi cantilever. The etching with 5%:30%:65% HF:HNO_3:H_2O of the 30 µm thick TiNi sheet resulted in a 7 µm undercut (left inset) and a conical side profile (right inset).

material to etch through 50 µm thick bulk TiNi material. Furthermore, for each of the materials four different HNA concentrations were tested to identify the most suitable concentration in terms of etch speed and quality.

The tested masking materials were photoresists, sputtered gold and PECVD deposited SiO_2 and Si_3N_4. The tested photoresist were both a positive and a negative resist, with a thickness of 1.2 µm and 2.8 µm, respectively. A hexamethyldisilane (HMDS) adhesion promoter was used and the resists were heat treated according to the manufacturers processing guidelines. The gold was 200 nm thick and sputtered onto the SMA after sputtering a 50 nm thick TiW adhesion layer, which is necessary to avoid delamination of gold from the SMA [28]. The PECVD layers were tested since they potentially allow to provide both a hardmask for the TiNi etching as well as the cold-state reset layer.

Table I overviews the tested materials, HNA concentrations and the obtained results. The experiments show that both photoresists were heavily attacked by the HNA etch solution. The positive resist completely delaminated for all concentrations of HNA while the negative resist proved some durability for low concentrations of HF, however, it was still found to be unusable as a masking material. The PECVD deposited SiO_2 and Si_3N_4 films were etched with an unacceptably low selectivity towards the bulk TiNi sheet. The gold was not etched at all and therefore identified as the best suited masking material, which is in agreement with previous work [28], [30].

Furthermore, the HNA concentration 5%:30%:65% HF:HNO_3:H_2O was found to be optimal in terms of limited HF exposure, controllable etch rate (approximately 10 $\mu m/min$) and acceptable conical etch profile with 7 µm undercut for a 30 µm deep etch (Figure 4).

C. Handling of patterned TiNi sheets

Patterning the TiNi sheet prior to bonding requires a temporary carrier substrate for the handling of the thin TiNi sheet during lithography and wet etching. The carrier substrate can be any substrate that withstands the TiNi etchant and allows for the necessary process steps such as resist spinning, lithography and etching. In this work, the carrier substrate was a thermally oxidized silicon wafer. However, the main challenge is to find a method for the temporary bonding of the TiNi sheet to the carrier substrate. The temporary bond must release the patterned TiNi sheet with limited mechanical stresses, since the thin sheet is fragile.

In this work, several methods were tested to temporarily bond the TiNi sheet to the carrier wafer. The tested bonding layers were positive photoresist, thermal release bonding sheets (Nitto Denko Revalpha) and dicing blue tape (Nitto Denko SWT 10+).

For testing the photoresist, the TiNi sheet was bonded to a 4 µm thick, softbaked (90 °C for 30 s) resist layer and the stack was then further baked (90 °C for 1 min] before patterning the TiNi sheet using lithography and HNA wet etching. However, during the HNA etching, the exposed bonding resist delaminated and contaminated the etchant. After the etching, the resist did not fully dissolve in Acetone and the patterned sheet had to be pulled off from the bonding layer, destroying the thin structures. Hence, photoresist was considered unsuitable for the process.

The thermal release sheets feature an adhesive layer on both sides, allowing to bond the TiNi sheet to the carrier wafer. After bonding and wet etching the TiNi, heating the stack above 90 °C should release the TiNi sheet from the thermal release sheet. However, the TiNi sheet was still softly bonded after heating and had to be pulled off, which destroyed the fragile TiNi structures. Hence, thermal release sheets were judged to be not suitable for the desired process.

Finally, standard 65 µm thick dicing blue tape was tested as illustrated in Figure 5a. The TiNi sheet was applied on the adhesive side of the blue-tape. Then, the TiNi/blue-tape stack

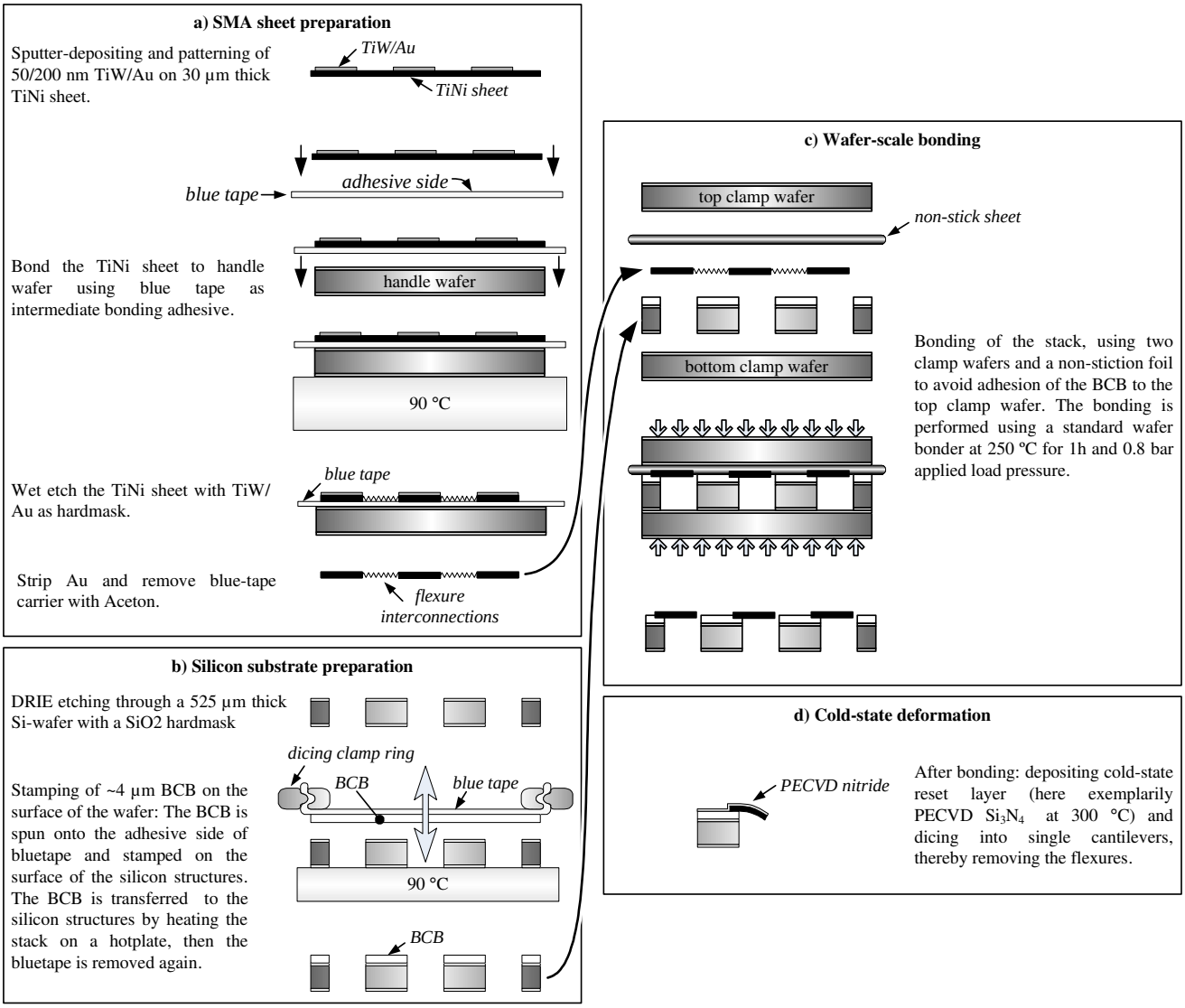

Figure 5. Outline of the process flow for the first demonstrators.

was applied onto the handle wafer with the non-adhesive side of the blue-tape facing the handle wafer. The complete stack was then placed for 5 s on a hotplate at 90 °C, causing a local melting of the blue tape at the interface to the Si wafer and adhesion of the blue-tape to the handle wafer. Next, the TiNi was patterned using lithography and wet etching. The blue-tape was found to withstand the TiNi etchant and to provide an excellent etch-stop. After the etching, the stack was placed in an Acetone bath to release the TiNi sheet from the blue-tape. Acetone causes swelling and softening of the blue-tape and the patterned TiNi sheet released from the stack without mechanical support. The TiNi sheet could be lifted off from the surface of the Acetone. Hence, blue-tape was judged to be a suitable temporary bonding layer for the etching of TiNi sheets prior to the adhesive bonding.

D. Optimization of transfer stamping adhesive on patterned silicon wafer

For the adhesive bonding of the TiNi sheet to a structured silicon wafer, BCB (Cyclotene 3022-46, DOW, USA) was chosen as the preferred adhesive because of its curing process that does not involve catalysts and thus no detectable outgasing of the polymer occurs after evaporating the solvents. However, since the wafer is patterned, the BCB cannot be spun onto the wafer. Spray-coating of the wafer with BCB is not applicable since this technique covers the sidewalls of etched features, which can destroy or block moving elements in the wafer. To transfer the adhesive onto the top surface of the silicon wafer only, the BCB was applied using an adapted contact printing (stamping) process, where the BCB is spun on an intermediate carrier substrate and then stamped onto the patterned target silicon wafer. In previous work [31], a thin layer of liquid BCB was transferred by stamping from a stiff auxiliary wafer substrate onto a patterned and hard-cured thick layer of BCB on the target wafer, followed by a separation through inserting

a razor blade inbetween the two wafers.

However, for the current work, the use of a stiff stamping wafer was found not suitable, mainly for two reasons. First, the area which should be covered with BCB was much larger as compared to the previous work, which made it very difficult to separate the two wafers after the stamping using the razor blade method. Instead, the wafers could only be separated by sliding, which smeared the BCB on sidewall features and resulted in a very inhomogeneous layer thickness. Secondly, as opposed to the BCB coated target in the previous work, the target here is a silicon wafer. Because the BCB adheres equally well to the stamp and the target, a repeatable and reliable layer transfer is difficult to achieve.

We circumvented these problems by using a flexible stamp instead. First, a polydimethylsiloxane (PDMS) film as intermediate substrate was tested, however, this process resulted in an incomplete BCB transfer with very inhomogeneous thicknesses. Then, standard 65 µm thick dicing blue tape was successfully tested as auxiliary substrate (Figure 5b). The blue tape was clamped in a standard 6 inch dicing ring and placed with the non-adhesive side on a 4 inch chuck of a standard resist-spinner. The BCB was spun onto the adhesive side of the blue-tape. Then the blue tape was placed with the BCB side on the target wafer and the whole stack was heated on a hotplate. The heat triggered a reflow of the BCB, which transferred fully to the target wafer, and released the blue tape, which could be lifted off simply from the stack. Upon inspection we verified that the BCB was transferred to all top parts of the silicon structures and no sidewall coverage could be observed.

IV. Fabrication and evaluation of first test structures

This section presents the fabrication and first evaluation of test actuator structures fabricated using wafer-scale integration of bulk TiNi material. The fabrication starts with the separate preparation of the TiNi sheet (Figure 5a) and the microstructured silicon wafer (Figure 5b).

A 30 µm thick TiNi sheet (Johnson-Matthey, USA, Ti 44.62 / Ni 55.37 weight %, A_f = 46.8 °C) was flattened by heating on a hotplate at 90 °C after which a 50/200 nm thick TiW/Au layer was sputter-deposited. The TiNi sheet was bonded to a temporary silicon handle wafer using blue-tape, as described above. Subsequently, the TiW/Au hardmask was patterned using standard positive lithography and wet etched to mask the outline of 2.5 mm long and 1 mm wide cantilever structures and their bond pads, interconnected with 100 µm wide flexure interconnections. Then, the exposed TiNi surface was wet etched. The Au was stripped off using iodine based etchant [30], leaving the TiW and the TiNi intact. Finally, the stack was put in Acetone to strip the photoresist and to release the TiNi sheet from the carrier substrate.

In parallel, a 525 µm thick silicon wafer was thermally oxidized and the oxide was patterned using lithography and wet etching in buffered hydrofluoric acid (BHF). Then, to allow the SMA microactuators to deflect freely during later operation, through holes were etched using deep reactive ion etching (DRIE) with oxide as etch mask. Subsequently, the

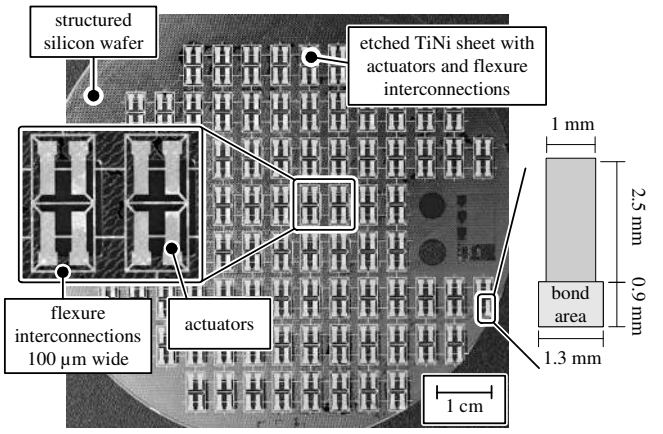

Figure 6. Photograph of the patterned TiNi sheet bonded to a structured silicon wafer. The blow-ups show the single actuator structures and the flexure interconnections as well as the outer dimensions of a single cantilever with its bond area.

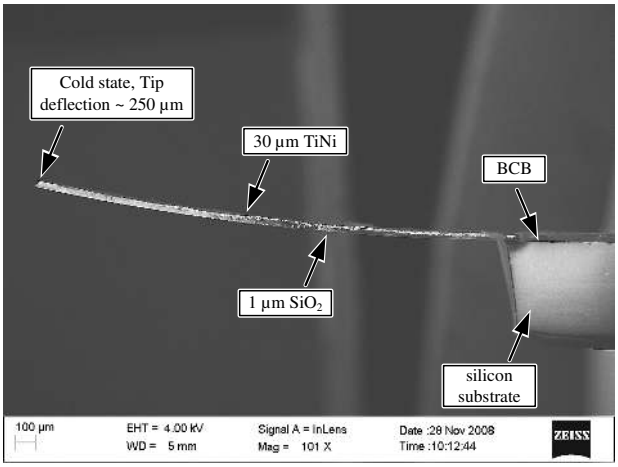

Figure 7. SEM-picture of a SMA microactuator structure in the cold-state.

BCB was stamped onto the top surface of the silicon wafer using the stamping technique described above.

Figure 5c illustrates the integration of the patterned TiNi sheet with the structured silicon wafer. The TiNi sheet was manually aligned to the structures of the silicon wafer and placed on the adhesive layer. To apply pressure while hard-curing the BCB, the stack was placed between two clamping wafers, with a teflon based non-stick sheet between the TiNi sheet and the top clamp wafer to avoid a bonding between the two. Then the stack was hard-cured in a wafer bonder during 1h at 250 °C and an applied load pressure of 0.8 bar. Figure 6 shows a photograph of the wafer/TiNi stack after bonding, including a blow-up of the cantilever structures and the flexure interconnections.

The final fabrication steps (Figure 5d) included the deposition of the cold-state reset layer and the dicing into single actuator structures, as described below.

After the fabrication, one wafer was diced in two halves using photoresist protection. On one half, a 1 µm thick compressively stressed PECVD Si_3N_4 layer was deposited at

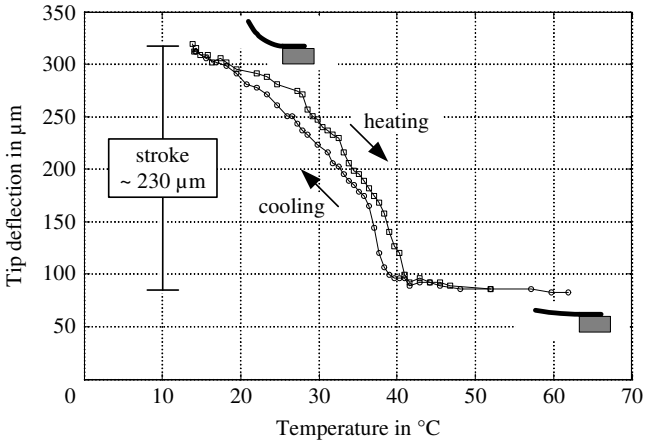

Figure 8. Tip deflection of a 2.5 mm long cantilever with 3 µm PECVD SiO_2at the backside versus hotplate temperature, displaying the SMA typical hysteresis behavior. In the cold/hot state, the tip deflection is approximately 315/85 µm, respectively, resulting in a stroke of 230 µm.

300 °C on the top side (Fig. 5d), resulting in a downward cantilever deflection of 125 µm in the cold-state and 28 µm in the hot-state, i.e. with a stroke of 98 µm. These results are corresponding to the theoretical tip deflections estimated in Figure 3.

The second half of the wafer was diced into single actuator structures, again using photoresist protection. All the structures survived the dicing and the correlated handling, including the post dicing Acetone stripping of the resist. Figure 7 shows a SEM picture of a structure with 1 µm PECVD SiO_2, deposited at 300 °C on the backside of the TiNi cantilever and providing an upward deflection. The cold-state and hot-state deflections were measured to 250 µm and 70 µm, respectively, resulting in a stroke of 180 µm. Figure 8 shows a temperature cycle measurement of another cantilever with 3 µm SiO_2 on the backside. The measurement shows that in the cold state the martensitic TiNi has a very low yield strength and is therefore easily deformed by the dominating thin stressing layer, resulting in a cold state tip deflection of 315 µm at 14 °C. However, in the hot state the TiNi is in the stiff austenitic state, dominating the deflection behavior by easily overcoming the bias spring force of the thin stressing layer and resulting in a nearly temperature-independent hot state deflection of 85 µm at 62 °C.

The measured deflections are corresponding to the estimations for the theoretical tip deflections in Figure 3. The stroke and the hysteresis show that the shape memory behavior of the TiNi is maintained during the integration process.

In another experiment the structure was placed on a hotplate and the cantilever tip was pushed downwards using an external manipulator. The temperature was cycled between temperatures below (30 °C) and above (70 °C) the transformation temperatures of the TiNi. By preventing the flat shape recovery of the cantilever, its leverage stresses the bond. The presented measurement proved that the bond is stronger than the forces created by the cantilever and the bond strength showed no degradation after more than 700 temperature cycles.

V. Conclusions

This paper presents a method for the wafer-scale integration of bulk TiNi based microactuators on silicon. The first bulk TiNi sheet based cantilevers, wafer-scale integrated on structured silicon wafers and with a cold state deformation provided by stressed layers, were shown. After an investigation of key process parameters, an optimized fabrication process was selected and demonstrated. 2.5 mm long cantilever test structures were evaluated and showed strokes of up to 230 µm, which is in agreement with the previous investigations. The bond strength proved to be stronger than the force created by the 2.5 mm long TiNi cantilever and showed no degradation after more than 700 temperature cycles. Moreover, the shape memory behavior of the TiNi is maintained during the integration process.

Acknowledgment

This work was part of the Q2M project. The authors would like to thank Johnson-Matthey, U.S., for providing the TiNi-sheets.

References

[1] D. Bell, T. Lu, N. Fleck, and S. Spearing, "MEMS actuators and sensors: Observations on their performance and selection for purpose," *Journal of Micromechanics and Microengineering*, vol. 15, no. 7, pp. 153 – 64, 2005/07/.

[2] E. Thielicke and E. Obermeier, "Microactuators and their technologies," *Mechatronics*, vol. 10, no. 4-5, pp. 431 – 455, 2000.

[3] M. Kohl, *Shape Memory Microactuators*. Springer, 2004.

[4] P. Krulevitch, A. Lee, P. Ramsey, J. Trevino, J. Hamilton, and M. Northrup, "Thin film shape memory alloy microactuators," *Journal of Microelectromechanical Systems*, vol. 5, no. 4, pp. 270 – 82, December 1996.

[5] W. Benard, H. Kahn, A. Heuer, and M. Huff, "Thin-film shape-memory alloy actuated micropumps," *Journal of Microelectromechanical Systems*, vol. 7, no. 2, pp. 245 – 51, 1998/06/.

[6] M. Kohl, D. Dittmann, E. Quandt, B. Winzek, S. Miyazaki, and D. M. Allen, "Shape memory microvalves based on thin films or rolled sheets," *Materials Science and Engineering A*, vol. 273-275, pp. 784 – 788, 1999.

[7] S. Takeuchi and I. Shimoyama, "A three-dimensional shape memory alloy microelectrode with clipping structure for insect neural recording," *Journal of Microelectromechanical Systems*, vol. 9, no. 1, pp. 24 – 31, 2000/03/.

[8] Z. Wei, R. Sandstrom, and S. Miyazaki, "Shape-memory materials and hybrid composites for smart systems. I. shape-memory materials," *Journal of Materials Science*, vol. 33, no. 15, pp. 3743 – 62, 1998/08/01.

[9] ——, "Shape memory materials and hybrid composites for smart systems. part II shape-memory hybrid composites," *Journal of Materials Science*, vol. 33, no. 15, pp. 3763 – 3783, 1998.

[10] K. Otsuka and C. Wayman, *Shape Memory Materials*. Cambridge University Press, 1998.

[11] D. Hodgson and J. Brown, "Using Nitinol alloys," Shape Memory Applications, Inc., White paper, 2000.

[12] A. D. Johnson, V. Martynov, and V. Gupta, "Applications of shape memory alloys: advantages, disadvantages, and limitations," vol. 4557, no. 1. SPIE, 2001, pp. 341–351.

[13] K. Skrobanek, M. Kohl, and S. Miyazaki, "Stress-optimised shape memory microvalves," in *Micro Electro Mechanical Systems, 1997. MEMS '97, Proceedings, IEEE., Tenth Annual International Workshop on*, 1997, pp. 256–261.

[14] S. Miyazaki, M. Tomozawa, and H. Kim, "Development of high-speed microactuators utilizing sputter-deposited tini-base shape memory alloy thin films," in *Proceedings ACTUATOR*, 2008, pp. 372–377.

[15] T. Mineta, K. Kasai, Y. Sasaki, E. Makino, T. Kawashima, and T. Shibata, "Flash-evaporated TiNiCu thick film for shape memory alloy micro actuator," *Microelectronic Engineering*, vol. 86, pp. 1274–1277, 2009.

[16] T. Grund, R. Guerre, M. Despont, and M. Kohl, "Transfer bonding technology for batch fabrication of sma microactuators," *Eur. Phys. J. Special Topics*, vol. 158, pp. 237–242, 2008.

[17] D. Clausi, H. Gradin, S. Braun, J. Peirs, G. Stemme, D. Reynaerts, and W. van der Wijngaart, "Microactuation utilizing wafer-level integrated SMA wires," in *Proceedings of the IEEE International Conference on Micro Electro Mechanical Systems (MEMS)*, 2009, pp. 1067–1070.

[18] N. Sandström, S. Braun, G. Stemme, and W. van der Wijngaart, "Full wafer integration of shape memory microactuators using adhesive bonding," in *Proceedings of the 15th international conference on solid-state sensors, actuators and microsystems (Transducers)*, 2009.

[19] M. J. Madou, *Fundamentals of Microfabrication*, 2nd ed. CRC Press LLC, 2002, ch. Surface Micromachining - Mechanical Properties of thin films, pp. 261–272.

[20] S. Prasanna and S. Spearing, "Materials selection and design of micro-electrothermal bimaterial actuators," *Journal of Microelectromechanical Systems*, vol. 16, no. 2, pp. 248 – 59, 2007/04/.

[21] F. Niklaus, G. Stemme, J. Q. Lu, and R. J. Gutmann, "Adhesive wafer bonding," *Journal of Applied Physics*, vol. 99, no. 3, p. 031101, February 2006.

[22] N. Sandström, S. Braun, G. Stemme, and W. van der Wijngaart, "Wafer-scale manufacturing of robust trimorph bulk SMA microactuators," in *Proceedings of the 11th international conference on new actuators (ACTUATOR)*, 2008, pp. 382–385.

[23] E. Suhir, "Predicted thermal stresses in a bimaterial assembly adhesively bonded at the ends," *Journal of Applied Physics*, vol. 89, no. 1, pp. 120 – 9, 2001/01/01.

[24] A. Tarraf, J. Daleiden, S. Irmer, D. Prasai, and H. Hillmer, "Stress investigation of PECVD dielectric layers for advanced optical mems," *Journal of Micromechanics and Microengineering*, vol. 14, no. 3, pp. 317 – 23, 2004/03/.

[25] Z. Cao and X. Zhang, "Mechanism of temperature-induced plastic deformation of amorphous dielectric films for MEMS applications," in *Proceedings of the 18th IEEE International Conference on Micro Electro Mechanical Systems (MEMS)*, 2005, pp. 471–474.

[26] J. Thurn and R. Cook, "Stress hysteresis during thermal cycling of plasma-enhanced chemical vapor deposited silicon oxide films," *Journal of Applied Physics*, vol. 91, no. 4, pp. 1988 – 92, 2002/02/15.

[27] J. Thurn, R. Cook, M. Kamarajugadda, S. Bozeman, and L. Stearns, "Stress hysteresis and mechanical properties of plasma-enhanced chemical vapor deposited dielectric films," *Journal of Applied Physics*, vol. 95, no. 3, pp. 967 – 76, 2004/02/01.

[28] J. Gill, K. Ho, and G. Carman, "Three-dimensional thin-film shape memory alloy microactuator with two-way effect," *Journal of Microelectromechanical Systems*, vol. 11, no. 1, pp. 68 – 77, 2002/02/.

[29] G. Kovacs, N. Maluf, and K. Petersen, "Bulk micromachining of silicon," *Proceedings of the IEEE*, vol. 86, no. 8, pp. 1536 – 51, 1998/08/.

[30] K. Williams, K. Gupta, and M. Wasilik, "Etch rates for micromachining processing-part II," *Journal of Microelectromechanical Systems*, vol. 12, no. 6, pp. 761 – 78, 2003/12/.

[31] J. Oberhammer and G. Stemme, "BCB contact printing for patterned adhesive full-wafer bonded 0-level packages," *Journal of Microelectromechanical Systems*, vol. 14, no. 2, pp. 419 – 25, 2005/04/.

Stefan Braun was born in Germany in 1980. He received the Dipl.-Ing. (FH) degree in microsystem technology from the University of Applied Sciences, Zweibrücken, Germany, in 2003. He is currently working toward the Ph.D. degree in the Microsystem Technology Laboratory, School of Electrical Engineering, KTH - Royal Institute of Technology, Stockholm, Sweden. He was with the Automotive Sensor Centrum, Robert Bosch GmbH, Reutlingen, Germany, where he worked with packaging aspects of inertial sensors and with ZF, Friedrichshafen, Germany, where he worked on finite-element simulations. His research interests include microelectromechanical systems switch arrays for automated telecommunication networks and the wafer-level heterogeneous integration of shape memory alloy actuator material.

Niklas Sandström was born in Sweden in 1981. He received the M.Sc. degree in engineering biology from Linköping University, Linköping, Sweden, in 2007. He is currently working towards the Ph.D. degree in the Microsystem Technology Laboratory, School of Electrical Engineering, KTH - Royal Institute of Technology, Stockholm, Sweden.

Göran Stemme (M'98-SM'04-F'06) was born in Stockholm, Sweden, in 1958. He received the M.Sc. degree in electrical engineering and the Ph.D. degree in solid-state electronics from Chalmers University of Technology, Gothenburg, Sweden, in 1981 and 1987, respectively.

In 1981, he was with the Department of Solid State Electronics, Chalmers University of Technology, where, in 1990, he was an Associate Professor (Docent), heading the silicon sensor research group. Since 1991, he has been with the Royal Institute of Technology, Stockholm, where he was a Professor and where he currently heads the Microsystem Technology Group, School of Electrical Engineering. His research is devoted to microsystem technology based on micromachining of silicon. His work spans a broad range of technological and application fields, such as medical technology, biochemistry, biotechnology, microfluidics, optical applications, wafer-level packaging, and device integration. Some of the results have successfully been commercialized. He has published more than 260 research journal and conference papers and has more than 22 patent proposals or granted patents. He has been a member of the Editorial Board of the *Journal of Microelectromechanical Systems* since 1997 and was a Member of the Editorial Board of the Royal Society of Chemistry journal *Lab on a Chip* from 2000 to 2005.

Dr. Stemme was a member of the International Steering Committee of the Conference series IEEE Microelectromechanical Systems between 1995 and 2001, and he was a General Cochair of that conference in 1998. In 2001, he was, together with two colleagues, the recipient of the final of the Innovation Cup in Sweden. He is a member of the Royal Swedish Academy of Sciences.

Wouter van der Wijngaart (M'06) received the M. Sc. degree in electrotechnical engineering, the degree of philosophic academy and the mathematics education degree, all from the Katholieke Universiteit Leuven, Belgium, in 1996 and the Ph. D. degree in Microsystem Technology from KTH - Royal Institute of Technology in Stockholm, Sweden, in 2002.

In 2005 he became Associate Professor and in 2007 Senior Lecturer with KTH Microsystem Technology Lab. His research focus is bio-, micro- and nanofluidics with a focus on lab-on-chip diagnostics and MEMS microactuators. He has over 70 scientific publications in the field. He is the co-founder of the company Easypark and at the base of the company MyFC, developing micro fuel cells for mobile applications.

Prof. van der Wijngaart was the ricipient of the Cap Gemini Innovation Award at the 1999 European Business Plan of the Year Competition in Paris, France, together with Fredric Ankarcrona, and the Swedish Innovation Cup 2001, together with Helene Andersson.